THE JOURNAL OF PHYSICAL CHEMISTRY C

Article

pubs.acs.org/JPCC

Iridium Oxidation as Observed by Surface Interrogation Scanning Electrochemical Microscopy

Netzahualcóyotl Arroyo-Currás and Allen J. Bard*

Center for Electrochemistry, Department of Chemistry and Biochemistry, The University of Texas at Austin, Austin, Texas 78712, United States

Supporting Information

ABSTRACT: The formation of surface oxides on most metal, including noble metal, electrodes occurs before the onset of the oxygen evolution reaction (OER). An understanding of changes in surface structure and composition caused by the oxidation process is important to the field of electrocatalysis of the OER. In this work, the surface interrogation mode of scanning electrochemical microscopy (SI-SECM) was used for the detection and quantification of $-OH_{(ads)}$ and $-H_{(ads)}$ species generated at the surface of polycrystalline iridium ultramicroelectrodes (UMEs) in 2 M NaOH. This system was selected because the iridium oxides are among the most effective and stable electrocatalysts for the OER. We introduce the redox pair Fe(III/II)−TEA as a mediator for stable surface interrogation at pH ≥ 12. This is the first time that SI-SECM experiments have been carried out at such an extreme pH. Monolayer coverage of $-OH_{(ads)}$ and $-H_{(ads)}$ was $Q_{\theta=1,OH}$ = 456 ± 2.0 μC cm^{-2} and $Q_{\theta=1,H}$ = 224.2 ± 0.2 μC cm^{-2}, respectively. At potentials more positive than 0.20 V, a clear change in the kinetics of the chemical reaction between Fe(II)−TEA and the hydrous oxides of Ir was observed. The kinetic results are interpreted with the aid of a simulation model based on finite element analysis (FEA). We present evidence that Ir(III), Ir(IV), and Ir(V) coexist on the surface of Ir during the OER under these conditions.

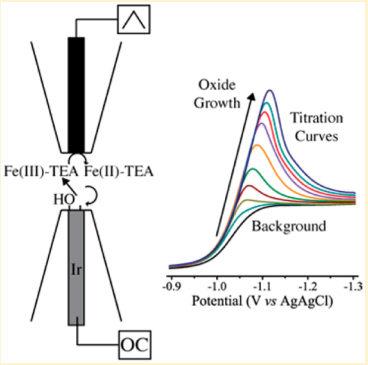

INTRODUCTION

The electrocatalytic oxidation of water is important in electricity- and light-driven water splitting devices.[1] Surfaces that promote the rate of water oxidation such as noble metal[2] and transition metal oxides[3] have been extensively studied. In fact, the electrocatalytic activity of noble metals is now generally attributed to the formation of surface oxides prior to the onset of water oxidation (generally called the oxygen evolution reaction (OER)).[4] A catalyst of particular interest is iridium oxide because of the low overpotential required to carry out the reaction (ca. 0.32 V) and because of its resistance to corrosion in a wide range of pH.[3,5] However, most of the research done on iridium oxides as electrocataysts for water oxidation has been devoted to the study of surfaces with thick oxide films. In this work, we present a different approach based on the study of the surface oxidation process starting with an oxide-free Ir(0) surface and systematically generating the incipient oxides over a potential window of 1.8 V, using the surface interrogation mode of scanning electrochemical microscopy (SI-SECM).[6] This approach facilitated the construction of titration curves that reveal all the surface transformations occurring on Ir under these conditions. We focused our efforts on the detection of oxide species with direct involvement in the OER.

Iridium oxide films are important in electrochemistry because of their applications to dimensionally stable anodes (DSA) for the OER,[7,8] their use as pH sensors *in vivo*,[9,10] and their electrocatalytic activity.[11] Surface characterization of iridium oxide films is typically carried out by voltammetry,[12−14] spectroscopy.[15,16] or a combination of both.[17] However, such approaches are not useful for the quantitative study of oxides at or below monolayer coverage, $\theta \leq 1$, for several reasons: (1) they are not sensitive enough;[18] (2) voltammetry uses the same surface to produce the incipient oxides and to detect them, potentially leading to convoluted results during analysis;[13] and (3) *ex-situ* techniques such as X-ray photoelectron spectroscopy (XPS) require ultrahigh vacuum that can induce chemical transformations of the sample. A recent paper[19] describes the use of *in situ* X-ray absorption spectroscopy (XAS) to study the oxidation states assumed by Ir in a thick oxide film during the OER. Although powerful, this technique still requires the use of thick oxide films. In contrast, SI-SECM offers several advantages for the study of incipient oxides at $\theta \leq 1$: (a) it is an *in situ* technique; (b) the sample electrode is decoupled from the probe electrode, minimizing unwanted perturbations of the sample during the detection step; (c) it is sensitive down to 3 to 4% monolayer coverage;[20] and (d) the time between generation and quantification of adsorbates can be optimized for the detection of short-lived species.[21] Furthermore, SI-SECM has been demonstrated to be a powerful tool for the study of adsorbed species and intermediates on noble metals.[20−23]

Received: January 5, 2015
Revised: March 24, 2015
Published: March 24, 2015

DOI: 10.1021/acs.jpcc.5b00106
J. Phys. Chem. C 2015, 119, 8147−8154

The most characteristic feature in voltammograms of anodically formed iridium oxide films is the quasi-reversible faradaic transition corresponding to Ir(III/IV),[17−25] at $E^{0\prime}$ = −0.40 V vs Ag/AgCl in 2 M NaOH (see trace **1** in Figure 1).

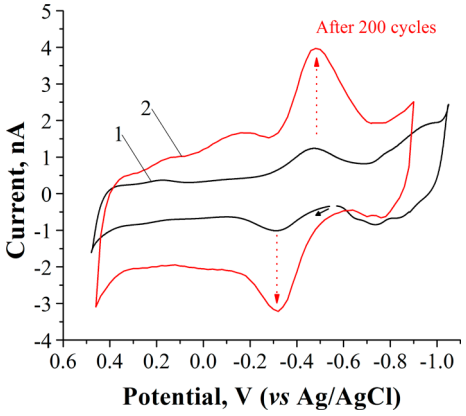

Figure 1. Cyclic voltammograms of Ir UMEs (a = 62.5 μm) in 2 M NaOH. (**1**) First scan over a clean, mirror-polished surface. (**2**) Last scan after the electrode was cycled between −0.85 and 0.48 V 200 times, v = 20 mV s^{-1}.

The determination of surface coverage on iridium requires precise control of the potential applied since thick-oxide growth occurs irreversibly at E > 1.1 V in 1 M H_2SO_4[12] or E > 0.4 V in 2 M NaOH. An example of a thick-oxide film grown on an Ir electrode is presented by trace **2** in Figure 1. Oxygen surface coverage up to θ = 1 was reported in 1.0 M H_2SO_4 to be Γ = 544 μC cm^{-2} from galvanostatic curves.[26] At potentials more positive than the Ir(III/IV) wave and θ = 1, Ir assumes oxidation states higher than Ir(IV), previously detected by XPS and XAS.[16,17] These higher oxidation state Ir oxides are believed to be key mediators in the electrocatalysis of the OER. Taking this into consideration, we carried out a systematic titration of Ir oxides by SI-SECM, starting from a clean surface of Ir(0). We focused our efforts on the detection of oxide species with direct involvement in the OER. We discuss our coulometry and kinetic data with the aid of numerical simulations based on finite-element analysis.

Mode of Operation. Scheme 1 describes the mode of operation of SI-SECM for the generation and titration of $-OH_{(ads)}$ on Ir. Henceforth, $-OH_{(ads)}$ represents any form of hydrous oxide present on the surface of Ir. The substrate is an Ir disk electrode surrounded by glass. The SI-SECM technique is divided in three steps as shown in Scheme 1. In the first step, a glassy carbon tip is aligned and approached to the Ir substrate, to d = 1−3 μm, under positive feedback conditions. In the second step, a potential is applied on the substrate (E_{subs}) for a characteristic time, t_{step}, to generate hydrous oxides, while the potential on the tip is at open circuit. In the third step, the potential of the substrate is taken to open circuit, and a cyclic voltammogram of the titrant, Fe(III)−TEA, is recorded on the tip. The potential waveform applied to the tip produces the reduced form of the titrant, Fe(II)−TEA, which diffuses toward the substrate and reacts with the hydrous oxides. Such a titration gives a transient positive feedback because Fe(II)−TEA is oxidized back to Fe(III)−TEA by $-OH_{(ads)}$. These reactions are written below

$$\mathrm{Fe(III)-TEA} + e^- \rightleftharpoons \mathrm{Fe(II)-TEA}, \quad E^{0\prime} = -1.05\ \mathrm{V} \tag{1}$$

Scheme 1. Description of the Surface Interrogation Technique for the Titration of $-OH_{(ads)}$ on Ir in 2 M NaOH[a]

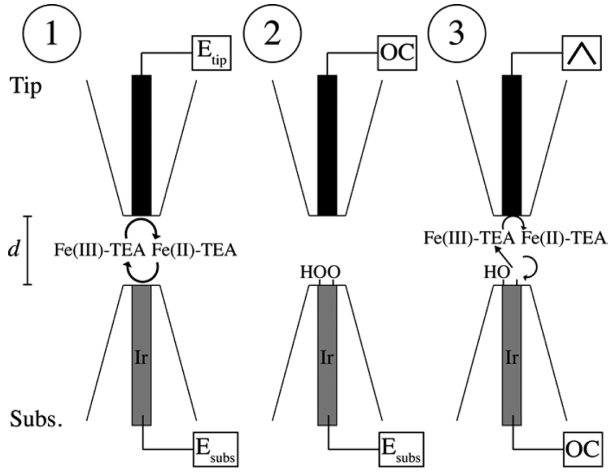

[a](1) Alignment, and approaching the tip to d = 1−3 μm from the substrate. (2) A potential E_{subs} is applied on the substrate, while the tip is at OC: Ir oxides are generated. (3) Titration of Ir oxides takes place by Fe(II)−TEA.

$$\mathrm{Fe(II)-TEA} + \mathrm{Ir-OH_{(ads)}} \overset{k_f}{\rightleftharpoons} \mathrm{Fe(III)-TEA} + \mathrm{Ir(0)} + \mathrm{OH^-} \tag{2}$$

Equation 2 is a generic expression representing the homogeneous electron transfer reaction between Fe(II)−TEA and hydrous oxides $Ir-OH_{(ads)}$, with rate of reaction k_f. The actual chemical formula of the oxide species produced in the interrogation experiment cannot be determined by SI-SECM.[20] When all the oxide species have reacted with Fe(II)−TEA, negative feedback behavior is observed, and the substrate electrode returns to its initial state. Figure 2 shows a characteristic voltammogram with feedback from the titration of oxides. Trace **1** in Figure 2 is a transient under negative

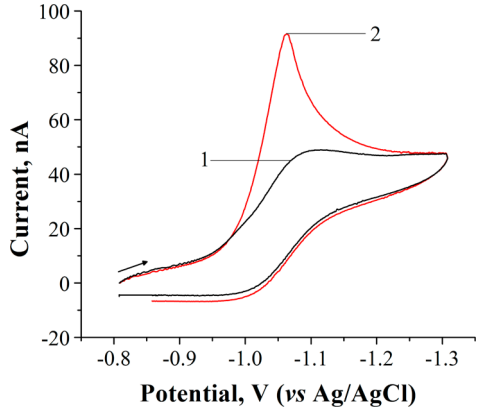

Figure 2. Cyclic voltammograms at a glassy carbon tip (a = 50 μm) in 5 mM Fe(III)−TEA + 2 M NaOH solution, during a titration experiment, with d = 2.8 μm and v = 10 mV s^{-1}. The substrate is an Ir electrode (a = 62.5 μm). (**1**) Voltammogram recorded in the absence of adsorbed species on the Ir substrate. (**2**) Interrogation transient obtained after generation of Ir oxides. The area under curve **2**, after subtraction of the black baseline, is divided by the scan rate at the tip to obtain the charge of adsorbates titrated during the experiment.

DOI: 10.1021/acs.jpcc.5b00106
J. Phys. Chem. C 2015, 119, 8147−8154

feedback conditions. Trace **2** in Figure 2 corresponds to a transient with feedback from adsorbed species.

EXPERIMENTAL SECTION

Reagents. All solutions were prepared in 2 M NaOH with Milli-Q water ($\rho \approx 18$ MΩ·cm). Solutions of ferrocenemethanol (FcMeOH) 97% from Sigma-Aldrich were prepared fresh prior to each experiment and were discarded after 4 h of preparation. The solutions of Fe(III)−TEA were prepared following a procedure described elsewhere.[27,28] Briefly, 20.0 mL of deionized water was poured into a round-bottom flask and bubbled with argon. After bubbling for 5 min, 4×10^{-4} moles of $Fe_2(SO_4)_3 \cdot 5\ H_2O$ from Acros Organics (Fair Lawn, NJ) were added with stirring. To this solution, 4.4×10^{-4} moles of triethanolamine (TEA) 98% from Sigma-Aldrich (St. Louis, MO) were added dropwise with stirring. In a separate container, NaOH pellets (0.08 mol) were dissolved in deionized water (10.0 mL) with stirring. After the NaOH dissolved, the container was placed in a water bath to cool at 25 °C. This NaOH solution was added dropwise to the Fe(III) + ligand solutions. The volume was adjusted to 40 mL upon completion of the synthesis reaction. The complex produced, $[Fe(TEA)(OH)]^-$, presents reversible electron transfer kinetics (ΔE_p = 60 mV, see Supporting Information SI-1) and is chemically stable in [NaOH] > 1 M. The formal reduction potential is $E^{0\prime} = -1.05$ V vs Ag/AgCl. The yield of the synthesis reaction was 95% as determined by steady-state voltammetry and the equation

$$\%\ \text{yield} = \frac{i_{ss,exp.}}{i_{ss,theo.}} \times 100 = \frac{i_{ss,exp.}}{4nFDCr} \times 100$$

where i_{ss} is the steady-state current from the experimental voltammogram; n is the number of electrons; F is Faraday's constant; D is the diffusion coefficient; C is the bulk concentration of Fe(III) used in the synthesis; and r is the radius of the UME. The diffusion coefficient was determined by the chronoamperometric method,[29] and a value of $D_{Fe(III)\text{-}TEA} = 2.0 \times 10^{-6}$ cm^2 s^{-1} was obtained. All chemicals were used as received.

Electrodes and SECM Cell. Iridium wire (99.9%, 125 μm diameter) from Alfa Aesar (Ward Hill, MA) was used to fabricate the substrate electrode by procedures described elsewhere.[30] A 100 μm diameter glassy carbon disk electrode was fabricated according to the procedure described in section SI-2 of the Supporting Information. All electrodes were polished prior to use with alumina paste on microcloth pads from Buehler (Lake Bluff, IL) and sonicated for 15 min in deionized water. Additionally, both substrate and tip electrodes were polished to RG = 1.1. All potentials in this work are reported vs the Ag/AgCl (1.0 M KCl) reference couple. A large surface area Pt mesh (Alfa Aesar) was used as the counter electrode. All solutions used in the electrochemical cell were bubbled with argon gas for 15 min prior to experimentation and were kept under a humidified argon blanket.

SI-SECM Routine. SECM and other electrochemical measurements were carried out with a CHI920C SECM station bipotentiostat and software from CH Instruments (Austin, TX). CH Instruments software allows the use of macro-commands to program instrumental routines. We created a routine to conduct SI-SECM experiments across a potential window of 1.80 V, every 0.01 V, with no intermissions (each instrumental routine ran for approximately 14 h, see Supporting Information SI-3). The experimental conditions were as follows: the potential of the substrate electrode was stepped at $E_{ini} = -1.00$ V for $t_{step} = 70$ s, after which it was immediately taken to open circuit. A resting time of $t_r = 2$ s was used between generation and interrogation. Then, cyclic voltammetry experiments were carried out at the tip electrode over a potential range between −0.85 and −1.30 V at a scan rate of ν = 10 mV s^{-1}. The magnitude of the potential step applied on the substrate electrode was changed by $\Delta E_{subs} = 0.01$ V after each experimental run, and the overall sequence was repeated to cover the range between $E_{fin} - E_{ini} = 1.80$ V. This is expressed algebraically as follows

$$\begin{aligned} E_{subs}(0) &= E_{ini} \\ E_{subs}(x) &= E_{ini} + x\Delta E_{subs} \\ E_{subs}(X) &= E_{fin} = E_{ini} + X\Delta E_{subs} \end{aligned} \tag{3}$$

where x is an integer such that $0 < x < X$ and $X = 180$ is the total number of increments. All experiments were carried out with 94% collection efficiency as determined by an independent tip generation−substrate collection (TG/SC) experiment using the couple FcMeOH/FcMeOH$^+$. Charge densities were determined from the interrogation transients, by integrating the area under the curve from each titration, then dividing by both the scan rate used at the tip and the area of the Ir electrode. A film of the native oxide was always present on the surface of the electrode before the first SI experiment. It was removed by titrating the surface with the strongly reducing titrant generated at the tip (E_{subs} = open circuit). After removal of the native film the electrode was kept at −1.0 V to prevent the formation of the first incipient oxides. This was done to ensure that the first titration experiment was carried out on a clean Ir(0) surface.

Numerical Simulations. We used numerical simulations to fit our experimental results. The digital model used is described elsewhere.[23] Briefly, the reaction Fe(III)−TEA + e ⇌ Fe(II)−TEA is considered at the tip, with forward, k_f, and reverse, k_b, rates of reaction defined according to the Buttler−Volmer formalism as

$$k_f = k^0 \exp^{[-\alpha f(E-E^0)]}$$

$$k_b = k^0 \exp^{[(1-\alpha) f(E-E^0)]}$$

where the heterogeneous rate constant is $k^0 = 6.3 \times 10^{-2}$ cm s^{-1};[31] α is the transfer coefficient (α = 0.5 in this work); $f = F/RT$; F is Faraday's constant; R is the gas constant; and T is the experimental temperature. The diffusion profile of electroactive species is calculated by solving Fick's second law in Cartesian coordinates for a two-dimensional geometry with axial symmetry. The net rate of chemical reaction between Fe(II)−TEA and $-OH_{(ads)}$ at the substrate electrode is defined as

$$k_{net} = \sum_j^0 k_j \Gamma_j C_{Fe(II)-TEA} \tag{4}$$

where k_j is the specific rate of chemical reaction between any single oxide of Ir and Fe(II)−TEA; Γ_j represents the surface concentration of $-OH_{(ads)}$ for an iridium oxide with oxidation state Ir^j; and $C_{Fe(II)\text{-}TEA}$ is the effective concentration of Fe(II)−TEA reacting with $-OH_{(ads)}$.

DOI: 10.1021/acs.jpcc.5b00106
J. Phys. Chem. C 2015, 119, 8147−8154

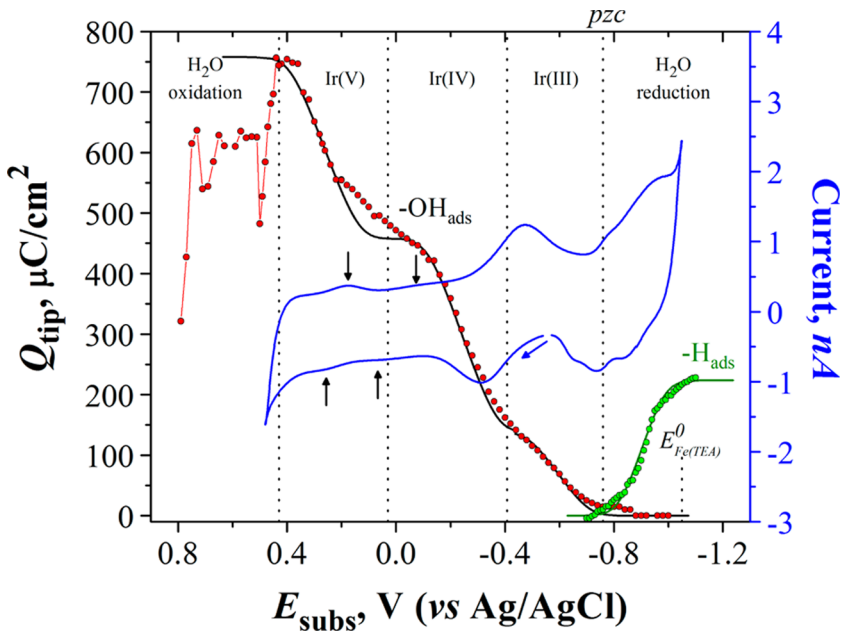

Figure 3. Plot of charge density, Q_{tip}, vs E_{subs} constructed from interrogation transients of $-OH_{(ads)}$ and $-H_{(ads)}$ adsorbed on Ir in 2 M NaOH. Red dots: $-OH_{(ads)}$, interrogated with 10 mM Fe(II)−TEA. E_{subs} was changed as indicated by eq 3 in the text. Green dots: $-H_{(ads)}$, interrogated with 1 mM $FcMeOH^+$. ΔE_{subs} = 0.01 V. Each dot is one individual SI-SECM measurement. Only a fraction of the data acquired is shown for clarity. Blue line: cyclic voltammogram of Ir UME (a = 62.5 μm) in 2 M NaOH, v = 20 mV/s. Black and green lines: fit of experimental data with Frumkin isotherms, using g' = −6 and g' = −2, respectively (Table 1). Red line: trace showing the order in which data were acquired at ΔE_{subs} > 0.44 V.

RESULTS AND DISCUSSION

Coulometry. *Monolayer Coverage of $-OH_{(ads)}$ and $-H_{(ads)}$.* The first detectable oxide of Ir in 2 M NaOH is seen at about −0.88 V (red circles in Figure 3), followed by oxide growth between −0.85 and −0.47 V. In this potential range, OH^- adsorbs on Ir, and the first hydrated oxides are formed.[32] Oxide coverage on the Ir substrate is θ < 1.0. The oxidation state of the atoms on the surface of the electrode is presumably Ir(III).[17] An inflection point is reached at E_{subs} = −0.40 V, with $Q_{\theta<1,OH}$ = 148 ± 2.0 μC cm^{-2}. The substrate potential where the inflection point occurs matches with the onset of the Ir(III/IV) wave seen in CVs of Ir UMEs in 2 M NaOH (blue trace in Figure 3). At substrate potentials more positive than −0.40 V, two processes occur simultaneously: oxide coverage progressively increases to $\theta \approx$ 1.0, and Ir(III) is oxidized to Ir(IV).[15,33−35] Further, a second inflection point is observed in the titration curve at E_{subs} = 0.03 V, with $Q_{\theta=1,OH}$ = 456 ± 2.0 μC cm^{-2}. This inflection point corresponds to θ = 1.0. The magnitude of the charge density at the inflection point is 100 μC cm^{-2} lower than values previously reported by Dahms and Bockris[26] in sulfuric acid ($Q_{\theta=1,OH}$ = 544 μC cm^{-2}).

In the case of $-H_{(ads)}$, the first detectable hydrogen atoms adsorbed on Ir are seen at about −0.70 V (green circles in Figure 3). The titration was carried out using FcMeOH as the titrant. FcMeOH is not chemically stable in 2 M NaOH for long times. However, we obtained reliable interrogation data within the first 2 h after preparation of the solutions. A Pt UME (a = 50 μm) was used as the tip. The reaction can be expressed in general as

$$FcMeOH^+ + Ir{-}H_{(ads)} + OH^- \overset{k_h}{\rightleftharpoons} FcMeOH + Ir(0) + H_2O \quad (5)$$

In the potential range from −0.70 to −1.1 V, surface coverage increases until a monolayer of $-H_{(ads)}$ is completed, with $Q_{\theta=1,H}$ = 224.2 ± 0.2 μC cm^{-2}. This value is in agreement with previous determinations by Woods[36] ($Q_{\theta=1,H}$ = 218 μC/cm^2).

Potentials Where $-OH_{(ads)}$ and $-H_{(ads)}$ Coexist. The surface oxidation of Ir in 2 M NaOH commences at potentials just beyond the hydrogen adsorption region.[12] In fact, $-OH_{(ads)}$ and $-H_{(ads)}$ probably coexist in that region. To characterize the potential range where both adsorbates are simultaneously present on Ir, we carried out titration experiments at substrate potentials presumably close to the potential of zero charge, pzc. The pzc for the Ir−2 M NaOH system has not been reported previously. In addition, the pzc of a bare Ir surface does not correspond to the pzc of an adsorbate-modified Ir surface under the same conditions.[37] We propose that the pzc of the Ir−2 M NaOH system is located within the double-layer charging region at this pH, approximately between −0.75 and −0.85 V. This assumption seems adequate based on values previously reported from capacitance−potential curves recorded on single-crystal Ir surfaces.[38] In the lower right corner of Figure 3, a region is seen where the charge from the titration of $-OH_{(ads)}$ (red circles) overlaps with that obtained from $-H_{(ads)}$ (green circles), at $E_{subs} \approx$ −0.78 ± 0.06 V. A potential region of about 120 mV exists where both adsorbates are simultaneously present on the surface of Ir. The center of such a region is labeled as pzc in Figure 3 and matches the substrate potential where a transition between hydrogen adsorption and surface oxidation is seen on the CV of Ir UMEs in 2 M NaOH (blue trace in Figure 3). This overlap region differs from that seen with Pt, where a large double-layer region separates the initial surface reduction and oxidation processes. The coexistence of $Ir{-}OH_{(ads)}$ and $Ir{-}H_{(ads)}$ at low coverages suggests that the adsorbed species are not very mobile on the surface. Additionally, we evaluated the minimum surface concentration of $-OH_{(ads)}$ and $-H_{(ads)}$ detected in our experiments, by averaging the first three data points from the red and green titration curves and calculating standard deviations. We

DOI: 10.1021/acs.jpcc.5b00106
J. Phys. Chem. C 2015, 119, 8147−8154

Table 1. Parameters Related to the Frumkin Isotherms Shown in Figure 3[a]

Frumkin isotherm: $\beta_i C_i = [\theta/(1-\theta)]e^{-g'\theta}$, where $\beta_i = \gamma_{\pm}\cdot e^{nF/RT(E_{subs}-E^{0\prime})}$ and $g' = [(2g\Gamma_{\theta=1})/(RT)]$				
E_{subs} region	adsorbate	g'	$E^{0\prime}$	charge at inflection point
−0.40 to −0.88 V	$Ir(OH)_x^{(3-x)}$	−6	−0.58 V	$Q_{\theta<1,OH}$ = 148 ± 2.0 μC cm^{-2}
0.03 to −0.40 V	$Ir(OH)_x^{(3-x)}$ + $Ir(OH)_y^{(4-y)}$	−6	−0.23 V	$Q_{\theta=1,OH}$ = 456 ± 2.0 μC cm^{-2}
0.44 to 0.03 V	$Ir(OH)_y^{(4-y)}$ + $Ir(OH)_z^{(5-z)}$	−6	−0.26 V	$Q_{\theta>1,OH}$ = 757 ± 2.0 μC cm^{-2}
E_{subs} > 0.44 V	H_2O oxidation	-	-	$Q_{>0.4\ V}$ = 614 ± 96 μC cm^{-2}
−0.70 to −1.10 V	$IrH_n^{(n)}$	−2	−0.90 V	$Q_{\theta=1,H}$ = 224.2 ± 0.2 μC cm^{-2}

[a]Independent variables used to simulate the Frumkin isotherm: n = 1; $\Upsilon_{\pm,OH-}$ = 0.743 taken from ref 41; F = 96, 485 C mol^{-1}; R = 8.314 J K^{-1} mol^{-1}, and T = 298.15 K.

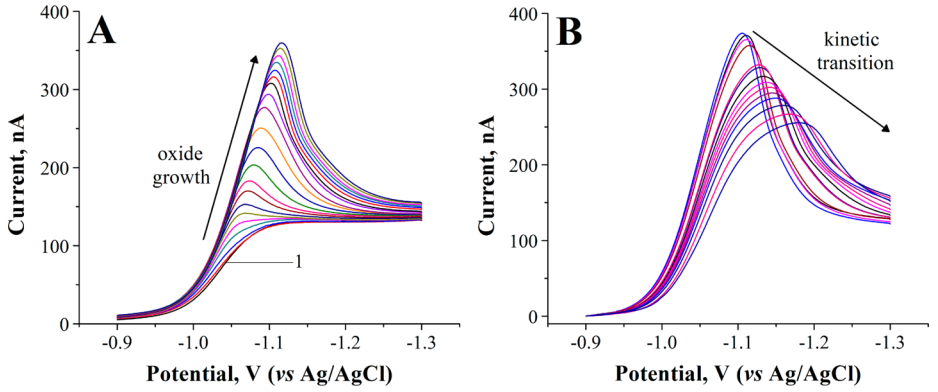

Figure 4. (A) Interrogation transients obtained in the range E_{subs} = −1.00 to 0.00 V. The transient labeled as **1** was recorded under pure negative feedback conditions. (B) Interrogation transients obtained in the range E_{subs} = 0.20−0.61 V. Only a few transients are shown for clarity. In all experiments: t_{step} = 70 s, t_{rest} = 2 s, and ν = 10 mV s^{-1}. Solution: 10 mM Fe(III)−TEA in 2 M NaOH. GC electrode (a = 50 μm).

obtained $Q_{min,H}$ = 0.93 ± 0.2 μC cm^{-2} for $H_{(ads)}$ and $Q_{min,OH}$ =11.4 ± 2.0 μC cm^{-2} for $-OH_{(ads)}$ or θ values of 0.01 for $H_{(ads)}$ and 0.025 for $-OH_{(ads)}$.

Iridium Oxides at θ > 1.0. Several small waves can be observed in the cyclic voltammograms of Ir in 2 M NaOH at E_{subs} > 0.03 V, shown by black arrows in Figure 3. Such processes are not evident in the first CV scan shown in Figure 3 (same as trace **1** in Figure 1) but become obvious after generation of a thick oxide film through potential cycling of the iridium electrode, as shown by trace **2** in Figure 1. The potentials at which those waves are observed in CVs coincide with an increase in charge density detected by SI-SECM. In the range −0.03 to 0.20 V, the slope of the titration curve presented in Figure 3 (red dots) is constant. This indicates that no faradaic process has occurred within the monolayer of oxide. Thus, the wave seen by CV in the same potential region can only be attributed to surface transformation processes, e.g., place exchange, slow oxide growth, and dehydration of $-OH_{(ads)}$ to $-O_{(ads)}$. However, when E_{subs} > 0.20 V the magnitude of the charge density integrated from SI-SECM transients sharply increases until a third inflection point is reached at E_{subs} = 0.44 V, with magnitude $Q_{\theta>1,OH}$ = 757 ± 2.0 μC cm^{-2}. From all the data presented so far, the following relationships become evident

$$\Delta Q_1 = Q_{\theta>1,OH} - Q_{\theta=1,OH} = 299 \pm 2.0\ \mu C\ cm^{-2} \quad (6)$$

$$\Delta Q_2 = Q_{\theta=1,OH} - Q_{\theta<1,OH} = 310 \pm 2.0\ \mu C\ cm^{-2} \quad (7)$$

$$\Delta Q_1 \approx \Delta Q_2 \quad (8)$$

Equations 6−8 clearly indicate that charge density determined by SI-SECM in the range 0.40−0.03 V is the same as the charge density determined in the range −0.40 to 0.03 V. Thus, the last inflection point (at 0.44 V) must correspond to a new faradaic conversion of Ir(IV) to Ir(V). The existence of Ir(V) oxides prior to the onset of the OER in sulfuric acid has been observed by XAS as reported elsewhere.[19]

The black trace in Figure 3 is a nonlinear fit of our $-OH_{(ads)}$ titration data with three contiguous Frumkin isotherms.[39,40] The green trace is a nonlinear fit of the $-H_{(ads)}$ data with a Frumkin isotherm. The isotherm equation used in this work is presented in Table 1. The parameters presented in Table 1 had the following definitions using $-OH_{(ads)}$ as an example: $\theta = Q_{Esubs}/Q_{\theta=1,OH}$ is the fractional coverage of the surface at a specific value of E_{subs}; $\Upsilon_{\pm}$ is the mean activity coefficient of OH^- extracted from the literature;[41] n is the number of electrons transferred; F is Faraday's constant; R is the gas constant; T is the absolute temperature; $E^{0\prime}$ is the formal reduction potential of the adsorbed species, taken as the $E_{1/2}$ in each charge transition from Figure 3; and g expresses the way in which increased coverage changes the adsorption energy $-OH_{(ads)}$. Parameters $E^{0\prime}$ and g were manually adjusted to achieve the best fit. The values used as inputs in the Frumkin isotherms are presented in Table 1. Interaction parameters g' = −6 and g' = −2 were used to fit the red and green data sets, respectively. In both cases, the negative magnitude of g' indicates repulsive interactions between the adsorbates.

Iridium Oxides after the Onset of Water Oxidation. When potentials more positive than E_{subs} = 0.44 V were applied to the Ir substrate, the SI-SECM titration recorded charge densities that are intermediate between oxides of Ir(IV) and Ir(V). In Figure 3, the charge integrated at E_{subs} > 0.44 V has an average magnitude of $Q_{>0.44\ V}$ = 614 ± 96 μC cm^{-2}. Note that the points overlaid with the red trace in Figure 3 are at midpoint between the inflection points at E_{subs} = 0.44 V and E_{subs} = 0.03 V. This result presumably indicates that Ir(IV) and Ir(V) oxides

DOI: 10.1021/acs.jpcc.5b00106
J. Phys. Chem. C 2015, 119, 8147−8154

coexist at E_{subs} > 0.44 V and are involved in the catalytic cycle of water oxidation in 2 M NaOH. Such a conclusion is further supported by analysis of the CV transients recorded during the titration experiments as discussed further in the following section. The same oxidation states of Ir have been observed by XAS in thick films immersed in acidic solutions during water oxidation.[19]

Kinetic Data. *Kinetic Behavior at 1.0 ≥ θ > 0.0.* Figure 4A presents interrogation transients recorded in the range −1.00 to 0.00 V. The first transient, labeled as **1** in Figure 4A, shows pure negative feedback because no $-OH_{(ads)}$ are generated on the surface of Ir at E_{subs} = −1.00 V. When E_{subs} is progressively stepped to more positive potentials, an interrogation peak starts to appear as the concentration of $-OH_{(ads)}$ increases on the surface of Ir. All the interrogation transients recorded in this potential range presented a similar shape, and the peak current progressively increased in magnitude. To better understand such a trend in oxide growth, we carried out numerical simulations and fit our experimental results with transients obtained from the FEA model. The overlap between experimental and simulated results is presented in Figure 5

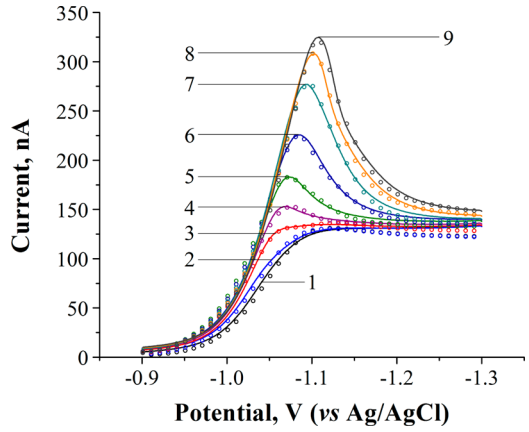

Figure 5. Numerical fit of experimental voltammograms from Figure 4A with simulated transients. E_{subs} was, from bottom to top: **1**, −1.00 V; **2**, −0.90 V; **3**, −0.80 V; **4**, −0.70 V; **5**, −0.60 V; **6**, −0.50 V; **7**, −0.40 V; **8**, −0.30 V; **9**, −0.20 V. v = 10 mV s^{-1}. The rate constant used to fit the data was $k_{IV,III}$ = 40 ± 5.0 mM^{-1} s^{-1}. The subscript in $k_{IV,III}$ refers to the oxidation states of Ir believed to exist when the titration was carried out, Ir(III) and Ir(IV).

(only a few transients are shown). In the numerical model, the only variable changed was the surface concentration of $-OH_{(ads)}$, Γ_j in eq 1. Three observations are important from these results: (1) the peak current is a function of the concentration of Ir(III) and Ir(IV) oxides on the surface of Ir; (2) the simulated rate constants k_{IV} and k_{III} have the same magnitude, $k_{IV,III}$ = 40 ± 5.0 mM^{-1} s^{-1}, also shown in Table 2, and are constant over the potential range considered; and (3) the peak potential of the interrogation transient shifts with increasing surface coverage. Such a shift in peak potentials has been discussed in previous reports[13,42] where surface oxidation of metals was studied by voltammetry and is generally attributed to adsorption/desorption kinetics of OH^- and to reorganization processes of the metal surface.

Table 2. Definition of Rate Constants in Terms of Process of Interest

rate constant	process	magnitude
k_{III}	titration of Ir(III)−$OH_{(ads)}$	40 ± 5.0 mM^{-1} s^{-1}
k_{IV}	titration of Ir(IV)−$OH_{(ads)}$	40 ± 5.0 mM^{-1} s^{-1}
k_V	titration of Ir(V)−$OH_{(ads)}$	15 ± 5.0 mM^{-1} s^{-1}

Kinetic Behavior at θ > 1.0. The interrogation transients obtained at potentials more positive than E_{subs} = 0.20 V present slower kinetics than those observed at θ ≤ 1.0 (Figure 4B). To better understand the nature of such changes in kinetic behavior, we modified the potential step condition at the substrate electrode from t_{step}= 70 s to t_{step}= 50 s to change the time dependence of our SI-SECM titrations. In essence, decreasing the perturbation time t_{step} limited the extent of surface reorganization (homogenization) happening before the interrogation of adsorbates. The goal was to detect individual trends of oxide growth at potentials more positive than E_{subs} = 0.00 V. Figure 6 shows the transients obtained after

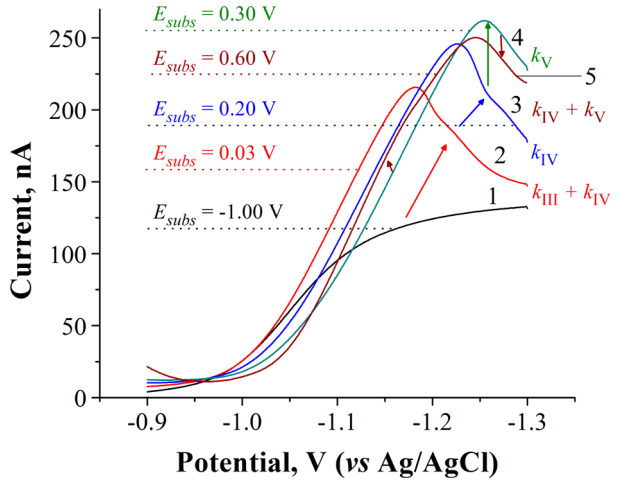

Figure 6. Interrogation transients obtained after modification of the potential step condition from t_{step}= 70 s to t_{step}= 50 s. Changes in E_{subs} caused shifts in peak potentials and changes in the shape of the interrogation transients. Glassy carbon tip electrode (a = 50 μm) and Ir substrate (a = 62.5 μm diameter); 10 mM Fe(TEA) in 2 M NaOH; v = 10 mV s^{-1}.

modification of t_{step}. In the figure, transient **1** is the negative feedback baseline. Transient **2** was obtained after setting E_{subs} = 0.03 V and presents a shape similar to those observed in Figure 4A. The rates of reaction corresponding to this transient are k_{III} and k_{IV} as mentioned before. However, at more positive potentials the kinetic regime changes. For instance, transient **3** in Figure 6 defines the limit in E_{subs} where kinetics are only controlled by rate k_{IV}, with a shift in peak potential of 44 mV more negative (blue arrow) than transient **2**. At E_{subs} > 0.20 V, new adsorbates are generated, Ir(V) oxides, and the net rate of reaction between the Ir(IV/V) oxides and Fe(II)−TEA is k_{IV} + k_V. A clear demonstration of this is shown in Figure 7, where mathematical fitting of the interrogation transient obtained at E_{subs} = 0.25 V required the addition of a second reaction rate in the FEA model

$$k_{net} = k_V \Gamma_V C_{Fe(II)-TEA} + k_{IV} \Gamma_{IV} C_{Fe(II)-TEA} \quad (9)$$

where k_{IV} = 40 ± 5.0 mM^{-1} s^{-1}, k_V = 15 ± 5.0 mM^{-1} s^{-1}, and Γ_V = 0.2 Γ_{IV} (for subscript associations see Table 2). At E_{subs} = 0.30 V, transient **4** in Figure 6, the contribution of Γ_V > 0.2 Γ_{IV} and the peak current potential shifted 30 mV more negative and increased in magnitude. The generation of Ir(V) oxides on

DOI: 10.1021/acs.jpcc.5b00106
J. Phys. Chem. C 2015, 119, 8147−8154

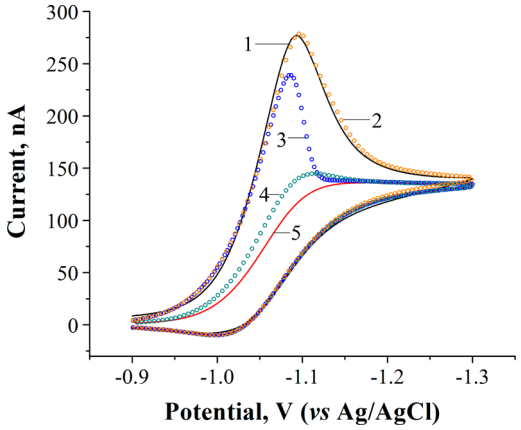

Figure 7. Theoretical fit of the interrogation transient obtained after holding the potential of the Ir substrate at E_{subs} = 0.25 V. (**1**) Experimental transient; (**2**) contribution of two species, $k_{IV}\Gamma_{IV} + k_V\Gamma_V$; (**3**) contribution of $k_{IV}\Gamma_{IV}$; (**4**) contribution of $k_V\Gamma_V$; (**5**) experimental transient obtained under negative feedback conditions.

the substrate is demonstrated by both coulometry and kinetic results.

Kinetic Behavior at E_{subs} > 0.44 V. When the Ir substrate is held at potentials where water oxidation actively occurs, the shape of the interrogation transients shows a behavior that is intermediate between Ir(IV) and Ir(V) oxides. This is shown by transient **5** in Figure 6, recorded after E_{subs} = 0.60 V was applied on the Ir substrate. In the figure, the dark red arrows point to a decrease in the peak current obtained from the surface titration and to a slight improvement in kinetics ($E_{1/2}$ = 20 ± 4 mV more positive, calculated from three repetitions) with respect to the green transient. The change in kinetics is small but reproducible. On the basis of the trends in reactivity observed so far, the change in kinetics at E_{subs} = 0.60 V does not indicate the appearance of a new oxide species (which would have $k < k_V$), but rather the average response of a new distribution of Ir(V) and Ir(IV) oxides on the surface of the substrate. We do not observe this behavior when carrying out the titration with t_{step} = 70 s, possibly because larger amounts of dissolved O_2 are produced and oxidize Fe(II)−TEA (increasing the extent of positive feedback at the tip). When the results from coulometry and the kinetic analysis are evaluated together, the OER on iridium oxides in 2 M NaOH probably follows the catalytic cycle expressed in eq 10

$$2\mathrm{Ir(V)} + 4\mathrm{OH^-} \rightleftharpoons 2\mathrm{Ir(III)} + 2\mathrm{H_2O} + \mathrm{O_2} \qquad (10)$$

where Ir(III) oxides generated from eq 10 are immediately converted to Ir(IV) and Ir(V) oxides at potentials E_{subs} > 0.44 V.

At substrate potentials E_{subs} > 0.60 V, dissolved O_2 accumulates in the gap between the two electrodes, and the SI-SECM titration becomes erratic. Occasionally, we observed formation of O_2 bubbles with consequent loss of current flow between the electrodes.

CONCLUSIONS

SI-SECM was employed to study the surface oxidation of polycrystalline iridium UMEs in 2 M NaOH. In particular, efforts were directed to understanding changes in the oxidation process prior to water oxidation. Several accomplishments are claimed in the present work:

- Fe(III/II)−TEA, a highly reducing mediator in strongly alkaline solution, was successfully used to carry out SI-SECM detection of $-OH_{(ads)}$ on Ir in 2 M NaOH.
- The potential of zero charge of the 2 M NaOH/H_2O/Ir system was characterized by SI-SECM, where adsorbed H and adsorbed OH coexist in small quantities.
- Quantitative determination of the charge density corresponding to one monolayer coverage of $-OH_{(ads)}$ and $-H_{(ads)}$ on Ir was performed. Values of $Q_{\theta=1,OH}$ = 456 ± 2.0 μC cm^{-2} for $-OH_{(ads)}$ and $Q_{\theta=1,H}$ = 224.2 ± 0.2 μC cm^{-2} for $-H_{(ads)}$ are reported in this work.
- Quantitative characterization of the main trends in surface oxide formation was achieved.
- Finally and more importantly, coulometric and kinetic evidence is provided for the coexistence of Ir(IV) and Ir(V) oxide species during the OER at pH = 14.

ASSOCIATED CONTENT

Supporting Information

Instructions for the fabrication of glassy carbon microelectrodes, as well as some experimental results relevant to this investigation. This material is available free of charge via the Internet at http://pubs.acs.org.

AUTHOR INFORMATION

Corresponding Author

*Phone: 512-471-3761. E-mail: ajbard@cm.utexas.edu.

Notes

The authors declare no competing financial interest.

ACKNOWLEDGMENTS

The information, data, or work presented herein was funded by the National Science Foundation (CHE-1111518) and the Welch Foundation (F-0021).

REFERENCES

(1) Trotochaud, L.; Ranney, J. K.; Williams, K. N.; Boettcher, S. W. Solution-Cast Metal Oxide Thin Film Electrocatalysts for Oxygen Evolution. *J. Am. Chem. Soc.* **2012**, *134*, 17253−17261.

(2) Damjanovic, A.; Dey, A.; Bockris, J. O. Kinetics of Oxygen Evolution and Dissolution on Platinum Electrodes. *Electrochim. Acta* **1966**, *11*, 791−814.

(3) Matsumoto, Y.; Sato, E. Electrocatalytic Properties of Transition Metal Oxides for Oxygen Evolution Reaction. *Mater. Chem. Phys.* **1986**, *14*, 397−426.

(4) Cook, T. R.; Dogutan, D. K.; Reece, S. Y.; Surendranath, Y.; Teets, T. S.; Nocera, D. G. Solar Energy Supply and Storage for the Legacy and Nonlegacy Worlds. *Chem. Rev.* **2010**, *110*, 6474−6502.

(5) McCrory, C. C. L.; Jung, S.; Peters, J. C.; Jaramillo, T. F. Benchmarking Heterogeneous Electrocatalysts for the Oxygen Evolution Reaction. *J. Am. Chem. Soc.* **2013**, *135*, 16977−16987.

(6) Rodríguez-López, J.; Zoski, C. G.; Bard, A. J. Application to Electrocatalysis and Photocatalysis and Surface Interrogation. In *Scanning Electrochemical Microscopy*, 2nd ed.; CRC Press: Boca Raton, 2012; pp 525−568.

(7) Beer, H. B. The Invention and Industrial Development of Metal Anodes. *J. Electrochem. Soc.* **1980**, *127*, 303C−307C.

(8) Ardizzone, S.; Trasatti, S. Interfacial Properties of Oxides with Technological Impact in Electrochemistry. *Adv. Colloid Interface* **1996**, *64*, 173−251.

(9) Papeschi, G.; Bordi, S.; Carlà, M.; Criscione, L.; Ledda, F. An Iridium-Iridium Oxide Electrode for *In Vivo* Monitoring of Blood *p*H Changes. *J. Med. Eng. Technol.* **1981**, *5*, 86−87.

(10) Macur, R. Iridium-Iridium Oxide Electrode for Measuring *p*H of Blood and Other Fluids. US Patent: US3726777 A, April 10, 1973.

DOI: 10.1021/acs.jpcc.5b00106
J. Phys. Chem. C 2015, 119, 8147−8154

(11) Buckley, D. N.; Burke, L. D. The Oxygen Electrode. Part 6. Oxygen Evolution and Corrosion at Iridium Anodes. *J. Chem. Soc., Faraday Trans. 1* **1976**, *72*, 2431−2440.
(12) Mozota, J.; Conway, B. E. Surface and Bulk Processes at Oxidized Iridium Electrodes. I. Monolayer Stage and Transition to Reversible Multilayer Oxide Film Behavior. *Electrochim. Acta* **1983**, *28*, 1−8.
(13) Stonehart, P.; Kozlowska, H. A.; Conway, B. E. Potentiodynamic Examination of Electrode Kinetics for Electroactive Adsorbed Species: Applications to the Reduction of Noble Metal Surface Oxide. *Proc. R. Soc. A* **1969**, *310*, 541−563.
(14) Chen, H.; Trasatti, S. Cathodic Behavior of Iridium Dioxide Electrodes in Alkaline Solution. Part I. Electrochemical Surface Characterization. *J. Appl. Electrochem.* **1993**, *23*, 559−566.
(15) Koetz, R.; Lewerenz, H. J.; Brueesch, P.; Stucki, S. Oxygen Evolution on Ruthenium and Iridium Electrodes. XPS-Studies. *J. Electroanal. Chem.* **1983**, *150*, 209−216.
(16) Koetz, R.; Neff, H.; Stucki, S. Anodic Iridium Oxide Films. XPS Studies of Oxidation State Changes and Molecular Oxygen Evolution. *J. Electrochem. Soc.* **1984**, *131*, 72−77.
(17) Minguzzi, A.; Lugaresi, O.; Locatelli, C.; Rondinini, S.; D'Acapito, F.; Achilli, E.; Ghigna, P. Fixed Energy X-Ray Absorption Voltammetry. *Anal. Chem.* **2013**, *85*, 7009−7013.
(18) Skoog, D. A.; Holler, F. J.; Crouch, S. R. *Principles of Instrumental Analysis*, 6th ed.; Cengage Learning: Belmont, 2006.
(19) Minguzzi, A.; Lugaresi, O.; Achilli, E.; Locatelli, C.; Vertova, A.; Ghigna, P.; Rondinini, S. Observing the Oxidation State Turnover in Heterogeneous Iridium-Based Water Oxidation Catalysts. *Chem. Sci.* **2014**, *5*, 3591−3597.
(20) Rodriguez-Lopez, J.; Alpuche-Aviles, M.; Bard, A. J. Interrogation of Surfaces for the Quantification of Adsorbed Species on Electrodes: Oxygen on Gold and Platinum in Neutral Media. *J. Am. Chem. Soc.* **2008**, *130*, 16985−16995.
(21) Park, H. S.; Leonard, K. C.; Bard, A. J. Surface Interrogation Scanning Electrochemical Microscopy (SI-SECM) of Photoelectrochemistry at a W/Mo-$BiVO_4$ Semiconductor Electrode: Quantification of Hydroxyl Radicals during Water Oxidation. *J. Phys. Chem. C* **2013**, *117*, 12093−12102.
(22) Rodriguez-Lopez, J. Surface Interrogation Mode of Scanning Electrochemical Microscopy (SI-SECM): An Approach to the Study of Adsorption and (Electro) Catalysis at Electrodes. In *Electroanalytical Chemistry: A Series of Advances*; CRC Press: Boca Raton, 2012; Vol. *24*, pp 287−351.
(23) Rodríguez-López, J.; Minguzzi, A.; Bard, A. J. Reaction of Various Reductants with Oxide Films on Pt Electrodes as Studied by the Surface Interrogation Mode of Scanning Electrochemical Microscopy (SI-SECM): Possible Validity of a Marcus Relationship. *J. Phys. Chem. C* **2010**, *114*, 18645−18655.
(24) Augustynski, J.; Koudelka, M.; Sanchez, J.; Conway, B. E. ESCA Study of the State of Iridium and Oxygen in Electrochemically and Thermally Formed Iridium Oxide Films. *J. Electroanal. Chem.* **1984**, *160*, 233−248.
(25) Vertova, A.; Borgese, L.; Capelletti, G.; Locatelli, C.; Minguzzi, A.; Pezzoni, C.; Rondinini, S. Cavity Microelectrodes for the Voltammetric Investigation of Electrocatalysts: the Electroreduction of Volatile Organic Halides on Micro-Sized Silver Powders. *J. Appl. Electrochem.* **2008**, *38*, 973−978.
(26) Dahms, H.; Bockris, J.O'M. The Relative Electrocatalytic Activity of Noble Metals in the Oxidation of Ethylene. *J. Electrochem. Soc.* **1964**, *111*, 728−736.
(27) Bechtold, T.; Burtscher, E.; Gmeiner, D.; Bobleter, O. The Redox-Catalysed Reduction of Dispersed Organic Compounds: Investigations on the Electrochemical Reduction of Insoluble Organic Compounds in Aqueous Systems. *J. Electroanal. Chem.* **1991**, *306*, 169−183.
(28) Arroyo-Currás, N.; Hall, J. W.; Dick, J. E.; Jones, R. A.; Bard, A. J. An Alkaline Flow Battery Based on the Coordination Chemistry of Iron and Cobalt. *J. Electrochem. Soc.* **2015**, *162*, A378−A383.
(29) Denuault, G.; Mirkin, M. V.; Bard, A. J. Direct Determination of Diffusion Coefficients by Chronoamperometry at Microdisk Electrodes. *J. Electroanal. Chem.* **1991**, *308*, 27−38.
(30) Bard, A. J.; Mirkin, M. V. *Scanning Electrochemical Microscopy*, 2nd ed.; CRC Press: Boca Raton, 2012; pp 25.
(31) Wen, Y. H.; Zhang, H. M.; Qian, P.; Zhou, H. T.; Zhao, P.; Yi, B. L.; Yang, Y. S. A Study of the Fe(III)/Fe(II)−Triethanolamine Complex Redox Couple for Redox Flow Battery Application. *Electrochim. Acta* **2005**, *51*, 3769−3775.
(32) Angerstein-Kozlowska, H.; Conway, B. E.; Mozota, J. The Role of Ion Adsorption in Surface Oxide Formation and Reduction at Noble Metals: General Features of the Surface Process. *J. Electroanal. Chem.* **1979**, *100*, 417−446.
(33) Otten, J. M.; Visscher, W. Anodic Behavior of Iridium. II. Oxygen Coverage. *J. Electroanal. Chem.* **1974**, *55*, 13−21.
(34) Plichon, V.; Petit, M. A. Anodic Electrodeposition of Iridium Oxide Films. *J. Electroanal. Chem.* **1998**, *444*, 247−252.
(35) Burke, L. D.; Whelan, D. P. A New Interpretation of the Charge Storage and Electrical Conductivity Behavior of Hydrous Iridium Oxide. *J. Electroanal. Chem.* **1981**, *124*, 333−337.
(36) Woods, R. Hydrogen Adsorption on Platinum, Iridium, and Rhodium Electrodes at Reduced Temperatures and the Determination of Real Surface Area. *J. Electroanal. Chem.* **1974**, *49*, 217−227.
(37) Guerrini, E.; Trasatti, S. Recent Developments in Understanding Factors of Electrocatalysis. *Russ. J. Electrochem.* **2006**, *42*, 1017−1025.
(38) Soliman, K. A.; Kibler, L. A. Variation of the Potential of Zero Charge for a Silver Monolayer Deposited Onto Various Noble Metal Single Crystal Surfaces. *Electrochim. Acta* **2007**, *52*, 5654−5658.
(39) Delahay, P. *Double Layer and Electrode Kinetics*; Interscience Publishers: New York, 1965.
(40) Bard, A. J.; Faulkner, L. R. *Electrochemical Methods: Fundamentals and Applications*; Wiley: New York, 2001.
(41) Ferse, A. Numerical Values of Individual Activity Coefficients of Single-Ion Species in Concentrated Aqueous Electrolyte Solutions and the Attempt of a Qualitative Interpretation on a Model of Electrostatic Interaction. *J. Solid State Electrochem.* **2013**, *17*, 1321−1332.
(42) Gileadi, E.; Conway, B. E. Kinetic Theory of Adsorption of Intermediates in Electrochemical Catalysis. *J. Chem. Phys.* **1963**, *39*, 3420−3430.

DOI: 10.1021/acs.jpcc.5b00106
J. Phys. Chem. C 2015, 119, 8147−8154